

In Situ Forming, Silanized Hyaluronic Acid Hydrogels with Fine Control Over Mechanical Properties and In Vivo Degradation for Tissue Engineering Applications

Killian Flegeau, Claire Toquet, Gildas Rethore, Cyril d'Arros, Léa Messenger, Boris Halgand, Davy Dupont, Florent Autrusseau, Julie Lesoeur, Joëlle Veziers, Pascal Bordat, Anthony Bresin, Jérôme Guicheux, Vianney Delplace, Hélène Gautier, and Pierre Weiss*

In situ forming hydrogels that can be injected into tissues in a minimally-invasive fashion are appealing as delivery vehicles for tissue engineering applications. Ideally, these hydrogels should have mechanical properties matching those of the host tissue, and a rate of degradation adapted for neo-tissue formation. Here, the development of in situ forming hyaluronic acid hydrogels based on the pH-triggered condensation of silicon alkoxide precursors into siloxanes is reported. Upon solubilization and pH adjustment, the low-viscosity precursor solutions are easily injectable through fine-gauge needles prior to in situ gelation. Tunable mechanical properties (stiffness from 1 to 40 kPa) and associated tunable degradability (from 4 days to more than 3 weeks in vivo) are obtained by varying the degree of silanization (from 4.3% to 57.7%) and molecular weight (120 and 267 kDa) of the hyaluronic acid component. Following cell encapsulation, high cell viability (> 80%) is obtained for at least 7 days. Finally, the in vivo biocompatibility of silanized hyaluronic acid gels is verified in a subcutaneous mouse model and a relationship between the inflammatory response and the crosslink density is observed. Silanized hyaluronic acid hydrogels constitute a tunable hydrogel platform for material-assisted cell therapies and tissue engineering applications.

1. Introduction

Hydrogels are increasingly used in the biomedical field, especially as scaffolds for tissue engineering.^[1] The highly hydrated structure of hydrogels, which are water-swollen polymer networks, reproduces some of the features (e.g., water content, stiffness) of native extracellular matrices,^[2] and facilitates cell encapsulation and maintenance of cell viability.^[3] Among the different classes of hydrogels, in situ forming hydrogels are of particular interest as their precursor solutions can be easily injected as liquids in a minimally-invasive manner before gelation within the target tissue.^[4,5] Beyond injectability, in situ forming hydrogels can fill complex defects,^[6] exert a protective effect on cells against shear forces,^[4] and limit cell leakage in vivo.^[7] They have therefore been investigated to improve limited access surgery in various animal models of

Dr. G. Rethore, C. d'Arros, Dr. B. Halgand, Dr. F. Autrusseau, J. Lesoeur, Dr. J. Veziers, Prof. J. Guicheux, Dr. V. Delplace, Prof. H. Gautier, Prof. P. Weiss

Université de Nantes

ONIRIS

INSERM

Regenerative Medicine and Skeleton, RMeS, UMR 1229

1 Pl A Ricordeau, Nantes F-44042, France

E-mail: pierre.weiss@univ-nantes.fr

Dr. K. Flegeau, Dr. G. Rethore, C. d'Arros, Dr. B. Halgand,

Dr. F. Autrusseau, J. Lesoeur, Prof. J. Guicheux, Dr. V. Delplace,

Prof. H. Gautier, Prof. P. Weiss

UFR Odontologie

Université de Nantes

Nantes F-44042, France

Dr. K. Flegeau, Dr. L. Messenger, D. Dupont, Dr. P. Bordat, Dr. A. Bresin
HTL S.A.S

7 Rue Alfred Kastler Javené 35133, France

Dr. C. Toquet

Department of Pathology

University Hospital of Nantes

Nantes F-44042, France

Dr. G. Rethore, Dr. B. Halgand, Dr. J. Veziers, Prof. J. Guicheux,

Prof. P. Weiss

CHU Nantes

PHU4 OTONN

Nantes F-44042, France

J. Lesoeur, Dr. J. Veziers

SC3M

SFR Santé F. Bonamy

FED 4203

UMS Inserm 016

CNRS 3556

Nantes F-44042, France

Prof. H. Gautier

Université de Nantes

Faculté de Pharmacie

Laboratoire de Pharmacie Galénique

Nantes F-44042, France

 The ORCID identification number(s) for the author(s) of this article can be found under <https://doi.org/10.1002/adhm.202000981>

DOI: 10.1002/adhm.202000981

tissue injuries, such as the heart (ovine)^[8] or intervertebral discs (goat).^[9]

In situ forming hydrogels can be obtained by the formation of covalent or noncovalent bonds between polymer chains after the injection.^[5] Nonetheless, owing to their increased mechanical properties and improved stability, covalent-based systems are generally preferred for long-term biomedical applications.^[10] During the last decades, a variety of crosslinking mechanisms, such as radical polymerization, Michael-type addition, or Schiff base formation, has been developed for in vivo applications.^[11] Yet, so far, the clinical translation of most of these strategies has been slowed down by inherently limiting factors. Some systems require external stimuli to crosslink (e.g., photopolymerization), making them hardly compatible with in situ forming and minimally invasive strategies. Others (e.g., Michael addition, disulfide, Schiff bases) lack in vivo stability and can react with native proteins; whereas some (e.g., inverse electron-demand Diels–Alder) are limited to the design of soft gels (typically below 5 kPa).^[5,12,13] Consequently, there is still a need for in situ forming and biocompatible systems with mechanical tunability and in vivo stability/degradability.

Hybrid inorganic–organic hydrogels based on metal oxide networks have been proposed as alternatives to conventional approaches owing to their ability to set under physiologically relevant conditions via a reversible sol–gel process.^[14] Among the different metal oxides that can be grafted onto polymer backbones, silanol alkoxides, Si(OR)_n, are particularly suited for the design of in situ forming hydrogels, leveraging the reversible self-condensation of silanol moieties (Si–OH) into siloxanes (Si–O–Si) at neutral pH.^[15] The hydrogel simply forms upon pH neutralization prior to injection, conveniently avoiding any detrimental influence on living tissues.^[16] In addition, the tetravalence of the silicon atom leads to the potential formation of three covalent bonds, reinforcing the stability of the network through the formation of crosslinking nodes.^[14]

Our laboratory has previously developed in situ forming silanized gels based on hydroxypropyl methylcellulose (HPMC). These silanized HPMC (Si-HPMC) hydrogels were shown to effectively support the long-term viability of encapsulated cells,^[17] and enable the paracrine secretion of proregenerative factors^[17] to stimulate the regeneration of various tissues (e.g., articular cartilage,^[18] heart,^[19] and colon^[20]). Yet, Si-HPMC gels have weak mechanical properties, with a typical stiffness of 3 kPa,^[21] resulting from the limited tunability of the silanol substitution. Furthermore, the use of HPMC as a support polymer that is not naturally present in the body, results in materials with limited biodegradability and bioactivity.^[22] These observations prompted us to develop an alternative hybrid inorganic–organic hydrogel with tunable mechanical properties and associated tunable degradability.

We investigated the use of hyaluronic acid (HA) as a support polymer because it combines the simplicity of chemical modification with biocompatibility, biodegradability, and low toxicity of by-products.^[23,24] HA is a major component of the extracellular matrix and is known to regulate tissue homeostasis,^[25] cell homing,^[26] and inflammation^[27] by interacting with various cell surface receptors (e.g., CD44, RHAMM, ICAM-1).^[28] Hydrogels containing silanized HA have recently been reported in the literature; however, the reported systems used additional crosslinkers,

such as 1,4-Butanediol diglycidyl ether^[29] or tetraethoxysilane^[30] to form mechanically stable hydrogels, resulting in preformed hydrogels that cannot be used in the framework of in situ forming systems. In this study, we obtained for the first time in situ forming, silanized HA hydrogels with tunable mechanical and swelling properties by finely controlling the molecular weight (MW) and the degree of substitution (DS). Upon pH neutralization of Si-HA solutions, low-viscosity precursors are obtained and easily injected through 23 G needles prior to gelation. The precursor solutions can further be used as biomaterials or as cell delivery vehicles for tissue engineering applications with excellent cytocompatibility. Subcutaneously injected Si-HA hydrogels demonstrated crosslink density-dependent biodegradation as well as high biocompatibility and tissue integration. Interestingly, a correlation between the inflammatory response and the crosslinking density was observed, opening up interesting perspectives for the design of well-tolerated injectable hydrogels. Si-HA hydrogels are promising in situ forming systems with potential applications in tissue engineering.

2. Results and Discussion

2.1. Synthesis and Characterization of Si-HA Hydrogels

Rarely reported in the literature, biomacromolecule silanization allows the synthesis of additive-free, self-setting hydrogels that are attractive for tissue regeneration.^[16,31] In our laboratory, these hybrid organic–inorganic materials were previously developed through the covalent grafting of alkoxy-silanes to the hydroxyl groups of cellulose derivatives, yet with limited control over the biodegradability and mechanical properties.^[32] Here, we hypothesized that silanized HA gels with tunable mechanical properties and degradation profiles could be obtained by controlling the DS and MW of the single HA-silanol macromolecular component. We successfully synthesized silanized HA (**Figure 1A,B**) from two different MW (332 and 2240 kDa) and with silanol substitution ranging from 4.3% to 57.7% (**Figure 1C**). Under similar reaction conditions, modifying higher MW HA led to lower DS, with a maximum value of 40.0% versus 57.7%, for 2240 and 332 kDa, respectively. A similar trend was previously reported for the methacrylation of HA,^[33] and may be attributed to steric hindrance and chain entanglement.^[34]

Following precursor dissolution in alkaline medium and sterilization through 0.22 μm filters, homogeneous hydrogels could be obtained upon simple pH adjustment to physiological pH (**Figure 1D**). A minimum polymer concentration of 3% w/v was required to form hydrogels from low-silanized HA (i.e., DS = 4.3% and 9.7%). This concentration was kept constant throughout the study to specifically investigate the influence of the DS and MW. Using size exclusion chromatography (SEC), we investigated the effect of basic pH on Si-HA and showed that the MW decreased to 120 ± 24 and 267 ± 99 kDa, for initial MW of 332 and 2240 kDa, respectively (**Table S1, Supporting Information**). This was expected as alkaline conditions induce HA depolymerization via β-elimination reactions and stepwise degradation from the reducing end.^[35,36] In the following article, the MW will refer to the values measured after the synthesis and dissolution.

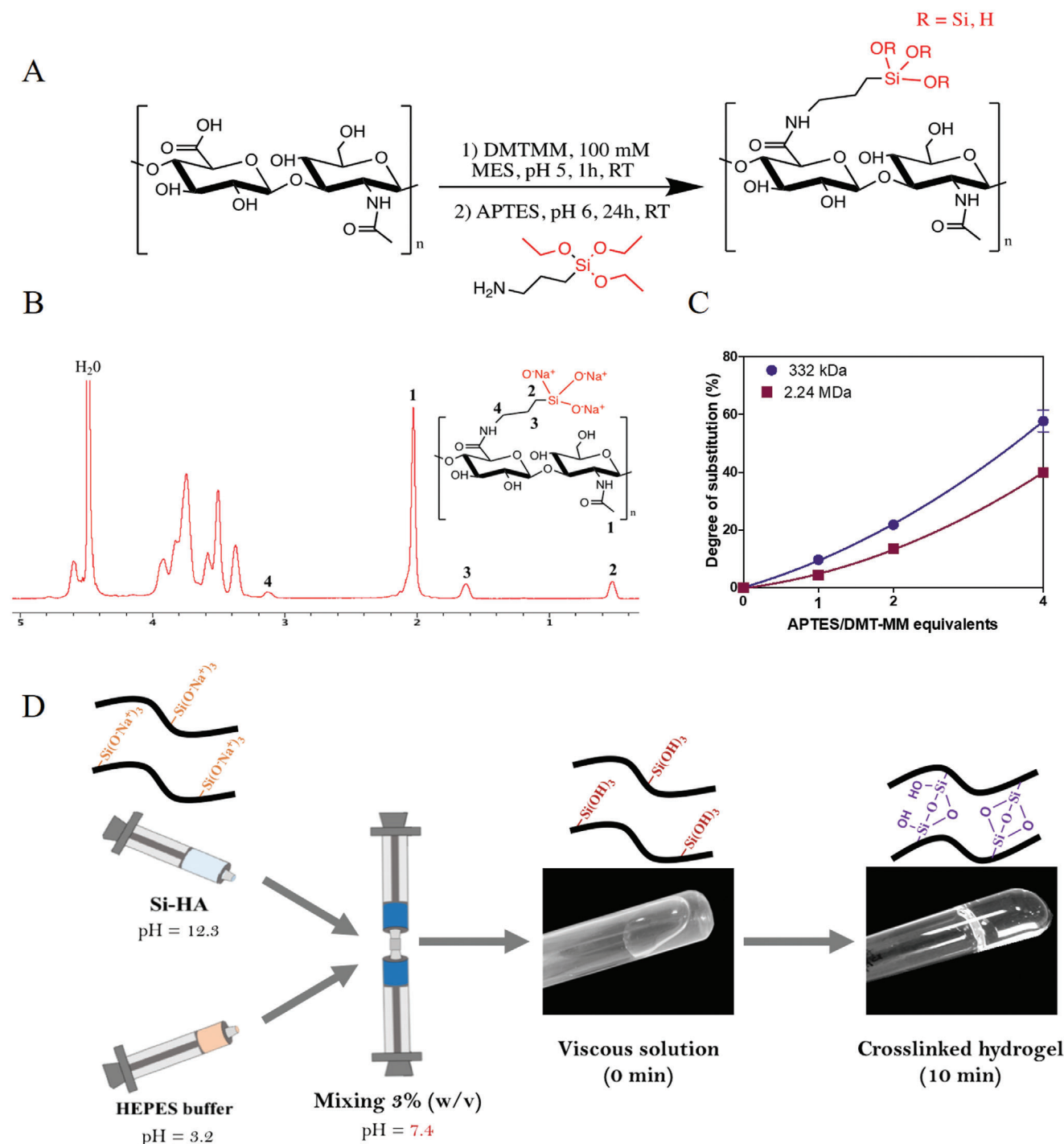


Figure 1. General strategy for the synthesis of Si-HA hydrogels. A) Synthetic route for the silanization of HA, using DMT-MM as the coupling agent and APTES as the aminoalkoxysilane. The synthesis is achieved in MES buffer at room temperature. B) Representative $^1\text{H-NMR}$ spectrum of Si-HA in NaOD, showing the successful grafting of silane moieties through the formation of the amide bond. Data are presented as mean \pm SD, $n = 3$. C) Degree of silanol substitution as a function of the HA MW and equivalents of APTES, as measured by ICP-AES. Data are represented as mean \pm SD, syntheses were tested in triplicates. D) Schematic of Si-HA hydrogel formulation: Si-HA dissolved in NaOH 0.1 N is mixed with an acidic buffer (HEPES, pH 3.2) using Luer-lock syringes, yielding injectable gel precursors within minutes at physiological pH. Hydrogels crosslink through the polycondensation of silanol moieties.

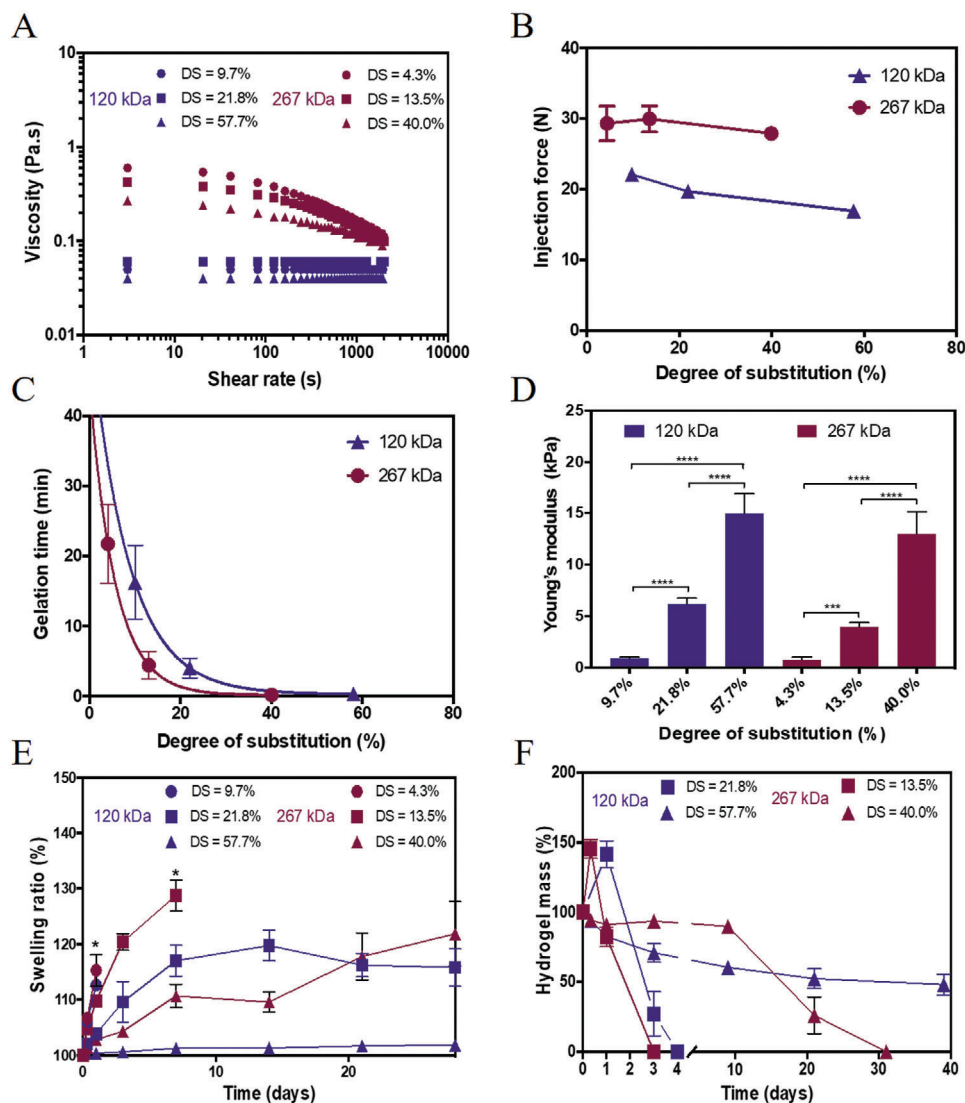


Figure 2. Physicochemical characterization of Si-HA hydrogels. A) Viscosity profile of Si-HA precursor solutions at 23 °C after 16 h dissolution in NaOH 0.1 N. B) Injectability of 3% w/v Si-HA precursor solutions through a 23 G syringe at room temperature. C) Gelation time of Si-HA solutions at 37 °C, representing the time when the loss tangent, $\tan \delta$, is independent from the 5 frequencies tested (0.1, 0.3, 0.5, 1.3, and 3 Hz), under a constant shear stress of 1 Pa. D) Young's moduli E) of Si-HA hydrogels as a function of the degree of substitution of HA-silanol. E) Equilibrium swelling (swollen mass/initial mass) of preformed Si-HA hydrogels in PBS at 37 °C. *indicates the last point before hydrogel collapse. F) Enzymatic degradation of Si-HA hydrogels in the presence of 10 U mL⁻¹ hyaluronidase at 37 °C. All the hydrogels were formulated at a 3% w/v concentration. Data are presented as mean \pm SD, $n = 3$. Statistical significance (D,E) was determined using a one-way ANOVA with a Tukey's multiple comparison test (ns: not significant, * $p < 0.05$, *** $p < 0.001$, **** $p < 0.0001$).

2.2. Injectability and Gelation Time of Si-HA Hydrogels

To evaluate if Si-HA hydrogels are compliant with minimally-invasive procedures, we first investigated the injectability of Si-HA hydrogels at physiological pH and room temperature. The viscosity of Si-HA precursors was assessed by rheometry at room temperature. All the Si-HA precursor solutions had low viscosity profiles, with zero-shear viscosities of 0.07 ± 0.006 Pa s and 0.63 ± 0.09 for MW of 120 kDa and MW 267 kDa, respectively (Figure 2A; and Table S1, Supporting Information). These low viscosity profiles were attributed to the reduced MW and the rupture of hydrogen bonds in alkaline environments.^[37] We further

evaluated the injectability of the Si-HA solutions by compression analysis after pH adjustment. A 23 G needle was chosen as it is commonly used in minimally-invasive approaches in preclinical animal experiments^[38] and in human clinical trials.^[39] The low viscosity of the Si-HA precursor solutions allowed their facile injection through the needle, with a maximal injection force of 30 ± 1.9 N, below the maximal manual injection force generally reported (≈ 30 –50 N) (Figure 2B).^[40] In anticipation of minimally-invasive surgeries, these results are highly encouraging as similar values were reported by Dolan et al., who injected HA-based hydrogels into porcine left ventricles through a minimally invasive procedure.^[41] By performing multifrequency sweep analysis,

the gelation time of Si-HA gels was next evaluated under physiological pH and temperature. Increasing the DS from 9.7% to 57.7% led to a decrease in gelation time from 16 min to ≈ 30 s, in a tunable fashion (Figure 2C). Increasing the MW from 120 to 267 kDa led to a similar decrease in gelation time, as reported by Cao et al., who found that an increase in the MW of HA from 0.1 to 2.0 MDa resulted in a concomitant decrease in the gelation time from 55 to 10.8 s.^[42] Controlling both the DS and MW allowed us to finely tune the gelation time, overcoming the common drawback of slow gelation rate associated with single-polymer crosslinking (e.g., disulfide bond).^[43] The silanization of HA is therefore an effective strategy to produce in situ forming hydrogels that are compliant with minimally invasive procedures, and should provide surgeons with convenient time to proceed with injections prior to in situ gelation.^[44]

2.3. Tunable Properties and Stability of Si-HA Hydrogels

We next studied the physicochemical properties of Si-HA hydrogels as a function of the DS and MW. By performing unconfined compression analyses, the elastic modulus of Si-HA hydrogels was first evaluated due to its central role in driving cellular behavior in vivo.^[45,46] Si-HA hydrogels showed Young's moduli ranging from 0.8 to 15 kPa, for DS ranging from 4.3% to 57.7% at 3% w/v (Figure 2D), and up to 40 kPa at 4% w/v (Figure S1, Supporting Information). This represents a significant increase as compared to previously synthesized Si-HPMC gels having a reported stiffness of 3 kPa.^[21] More importantly, the tunable stiffness of Si-HA hydrogels might be further used as a cell-instructive factor^[12] to favor cell differentiation, as reported by Engler et al. in their seminal study.^[47]

We then evaluated the swelling and stability of Si-HA hydrogels immersed in phosphate buffer saline (PBS) (Figure 2E). Low-silanized hydrogels (i.e., DS of 4.3% and 9.7%) swelled rapidly, and completely dissolved within 2 d, most likely due to an insufficient crosslink density. This limited stability was considered inadequate for biomedical applications, and the gels were not further analyzed in this study. Si-HA with a DS of 13.5% first swelled for 7 d ($128.8\% \pm 2.8\%$) before being progressively degraded. Using average silanol DS (21.8% and 40.0%), Si-HA gels swelled for 7 d before reaching a plateau with maximal values of $117.1\% \pm 2.8\%$ and $121.8\% \pm 5.8\%$ after 28 d, respectively. Highly silanized HA (DS = 57.7%) showed minimal to non-swelling ($101.8\% \pm 0.8\%$) after 28 d. These results indicate that the swelling profiles of Si-HA gels are ruled by the crosslink density. As a complementary analysis, the mesh size of the fully-swollen hydrogels were calculated according to the equations of Canal and Peppas,^[48] and was found to vary from 76 to 15 nm, for DS ranging from 21.8% to 57.7% (Figure S2, Supporting Information). These values are commonly reported in the literature and correspond to a porosity that should allow adequate nutrient diffusion throughout the gels.^[49] As a first evaluation of Si-HA gels degradability, we finally evaluated the degradation of Si-HA hydrogels in the presence of hyaluronidase at 37 °C (Figure 2F), using an enzyme concentration of 10 U mL⁻¹, as previously reported.^[33,50] For both MW (120 and 264 kDa), increasing the crosslink density resulted in slower gel degradation. Thus, low-DS hydrogels (DS = 9.7%) were fully degraded within 12 h,

whereas high-DS hydrogels (DS = 57.7%) had 50% of their initial masses remaining after 40 d. Interestingly, Si-HA gels with DS = 57.7% showed a fairly linear degradation profile, typical of a surface erosion mechanism.^[51] This degradation profile is rarely observed for hydrogels, which generally undergo bulk erosion.^[52] Conversely, Si-HA gels with DS = 40.0% showed limited degradation before 10 days, then rapidly degraded. This may reflect a switch from a surface to bulk erosion, where the diffusivity of water and enzyme become faster than bond cleavage.^[52] Such mechanism could have interesting applications for controlled delivery of molecules.^[52] The wide range of degradation times obtained in vitro constitutes a significant improvement as compared to most in situ gelling systems, for which degradation rates within hours to days are generally reported.^[53] Together, these results demonstrate that the crosslink density is a key parameter to control the stiffness, swelling, and stability of Si-HA gels. More importantly, these hydrogels were shown to combine proper injectability and tunable properties, which is highly relevant for tissue engineering applications.

2.4. Cytocompatibility of Si-HA Hydrogels

Hydrogels are generally regarded as cell-friendly materials; however, shear stress during the injection, traces of residual contaminants/solvents, or small pore size may affect cell viability.^[33,54] To evaluate the cytocompatibility of Si-HA gels, viability experiments were conducted over 7 d using an established murine fibroblastic cell line (L929) and two types of human stromal cells (hASCs and hBMSCs) often used in tissue engineering. Viability was evaluated using a Live/Dead assay and confocal imaging (Figure 3A–E). Actinomycin-D (an inhibitor of transcription) treatment was added as a negative control to confirm our ability to detect dead cells. In all the gel formulations tested, a high cell viability ($\geq 80\%$) was maintained over at least 1 week, with no significant difference between day 1, 3, and 7, confirming the cytocompatibility of the pH-triggered crosslinking reaction and that of the obtained gels. These results also indicate that the crosslink density, and thus the stiffness, does not markedly affect cell viability over the range tested. Similar observations were recently reported for hBMSCs encapsulated in gelatin gels with stiffness varying from 2 to 60 kPa.^[55] It is therefore likely that nutrients and oxygen diffusion and wastes removal operate, even in the highly silanized hydrogels (DS = 57.7%). L929 proliferated in small localized clusters at D7, which is a common behavior of L929 cells cultured in dynamic and nonadhesive environments.^[56,57] Interestingly, this observation also suggests that Si-HA gels form relatively permissive environments to cell proliferation, which is a feature rarely observed in covalent systems.^[13] Finally, as cells injected through a needle might experience mortality due to shear stress depending to the flow and viscosity behavior,^[58] we studied if hASCs would remain viable after injection in Si-HA precursor solutions through a 23G needle (Figure 3F). We showed that cells remain viable ($> 85\%$) in all the conditions, confirming that cells encapsulated in Si-HA gels are not affected by the injection process. Altogether, these results indicate that Si-HA hydrogels are cytocompatible vehicles for cell encapsulation and delivery.

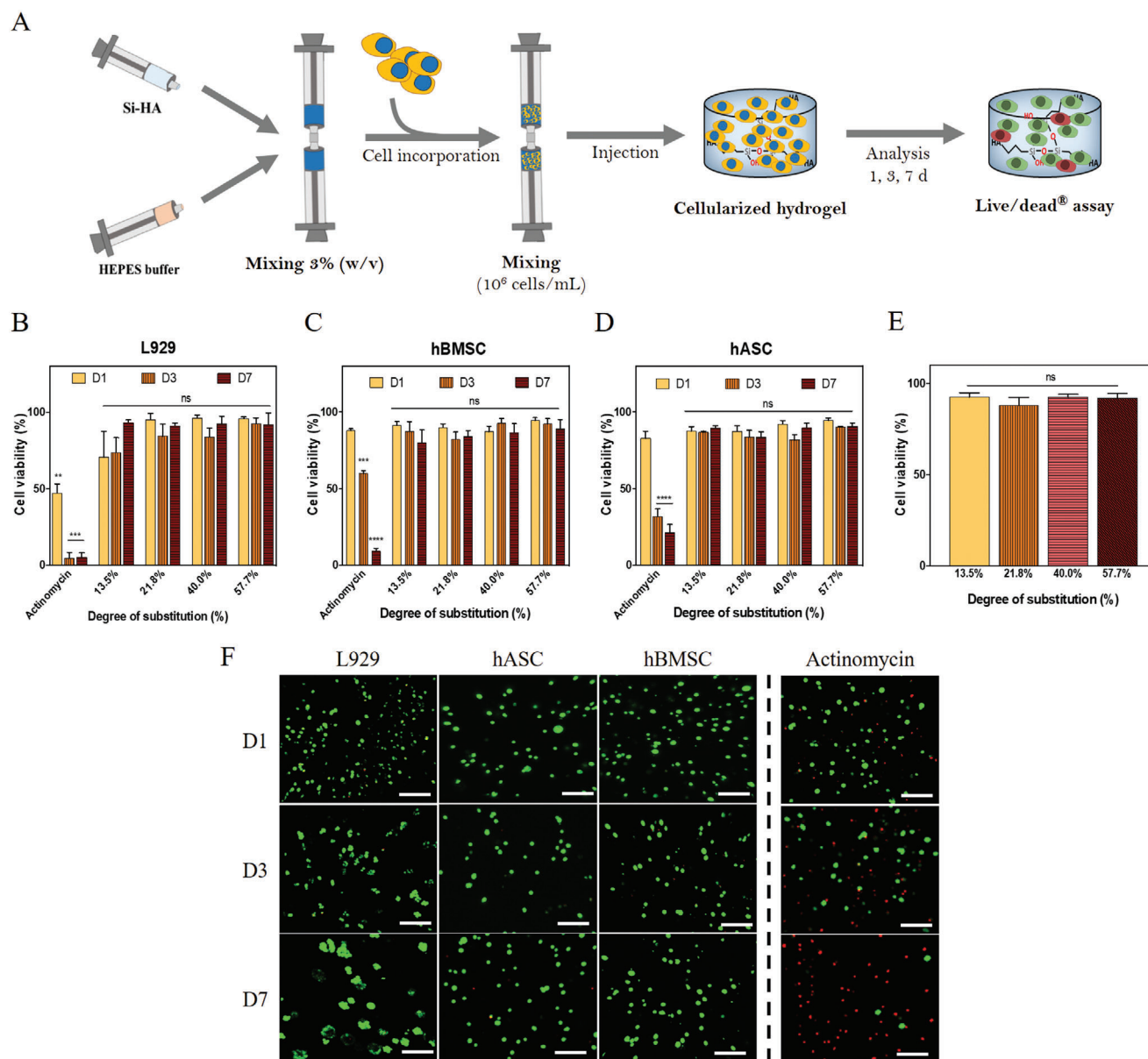


Figure 3. Cytocompatibility of Si-HA hydrogels. A) Schematic of Si-HA gels formulation and cell encapsulation: 10^6 cells mL^{-1} are incorporated after pH adjustment to 7.4 and homogenized by manual mixing with Luer-lock syringes before injection. The viability of L929 cells B), hBMSCs C), and hASCs D) encapsulated in 3% w/v Si-HA hydrogels, as a function of the degree of substitution of Si-HA (13.5%, vs 21.5% vs 40.0% vs 57.7%). Viability over time (1, 3, and 7 d) was determined using a live/dead assay, and calculated as the number of viable cells divided by the total number of viable and dead cells. E) Viability of encapsulated hASCs in Si-HA hydrogels (DS = 13.5%, 21.8%, 40.0%, and 57.7%) injected 1 min after pH adjustment and mixing with the cells, through a 23G needle. F) Representative images of a negative control (actinomycin-D) as well as hASCs, hBMSCs, and L929 incorporated in Si-HA hydrogels with DS = 40.0% over 7 d. Scale bar: 100 μ . Data are presented as mean \pm SD, $n = 3$ hydrogels with 3 random fields were taken for analysis. Statistical significance was determined using a one-way E) or two-way ANOVA B–D) with a Tukey's multiple comparison test. (ns: not significant, ** $p < 0.01$, *** $p < 0.001$, **** $p < 0.0001$).

2.5. In Vivo Degradability of Si-HA Hydrogels

Implanted hydrogels should ideally have tunable biodegradation kinetics profiles to either match the rate of neo-tissue regeneration,^[59] or to degrade in a controlled manner after completion of their initial objective (i.e., imaging, drug delivery).^[60,61] To evaluate the biodegradation properties of Si-HA hydrogels, various gel formulations (DS = 13.5–57.7%) were injected in the

subcutis of immunocompetent mice under aseptic conditions, and submitted to two volume assessment methods after 7 and 21 d. This model is particularly useful to obtain general information on degradation rates and inflammatory response following hydrogel injection, in anticipation of future applications in vascularized tissues.^[62] As a first semiquantitative approach, a daily palpation test was performed to assess the in vivo erosion of hydrogels over time (Figure 4A,C). On day 0, all the formulations

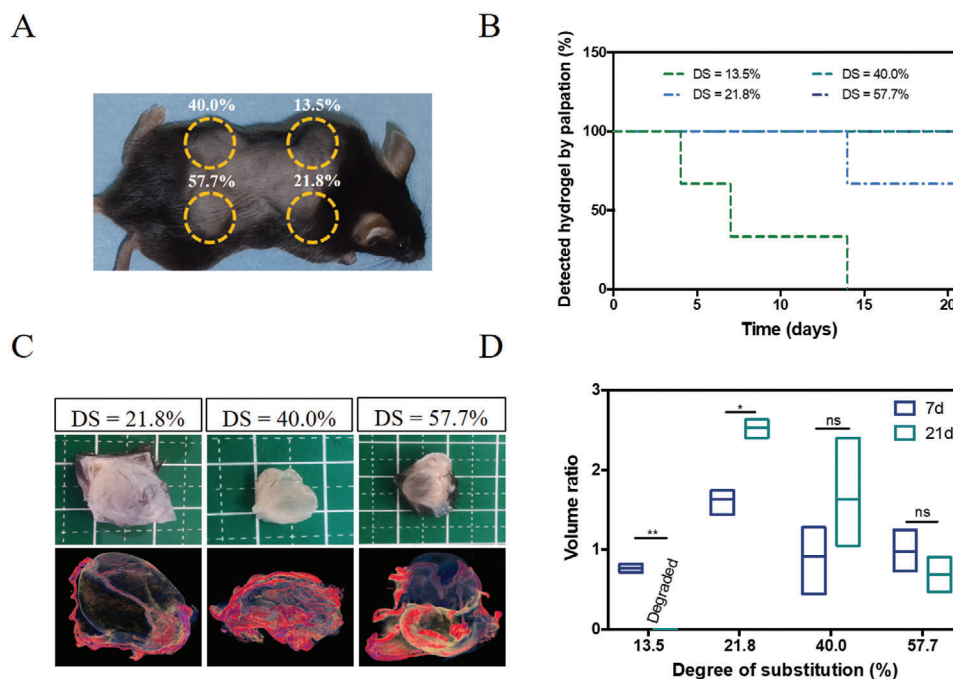


Figure 4. In vivo biodegradation of Si-HA hydrogels as a function of the crosslink density. A) Representative picture of a C57/BL6 mouse after the injection of Si-HA hydrogels. Dotted yellow circles indicate the injection areas. The DS of the injected hydrogel is indicated on top of the corresponding circle. B) Evaluation of the in vivo degradation of Si-HA gels over time, using palpation as a semiquantitative method. C) Representative images of the explanted gels (top) and stained samples (bottom), at 3 weeks after injection. D) Relative in vivo swelling of Si-HA hydrogels at 7 and 21 d after injection, as determined by microcomputed tomography. The samples were stained with phosphotungstic acid and analyzed by μ CT. Volumes were normalized to the injected volume of 250 μ L (represented by the dotted line). Data are represented as mean \pm SD, $n = 3$ implants. Statistical significance of volume variation between 7 and 21 d was assessed by an unpaired Student t -test D). (*, $p < 0.05$, ** $p < 0.01$).

tested led to gels that could be manually detected, confirming the successful in situ formation of Si-HA gels. For a DS of 13.5%, gels could no longer be detected by palpation after 4–14 days postinjection (Figure 4B), indicating rapid biodegradation in agreement with the limited stability observed in vitro. Increasing the DS to 21.8% yielded more stable hydrogels in vivo, with first signs of biodegradation occurring after 14 d. Gels from highly silanized components (i.e., 40.0% and 57.7%) were still intact after 21 d. To further assess their in vivo behavior, gels were explanted for μ CT analysis at 1 and 3 weeks after injection (Figure 4D). The volume of explanted samples after 7 and 21 d was calculated and compared to the initially injected volume of 250 μ L. Low silanized HA (DS = 13.5%) showed a volume reduction of $23.5\% \pm 7.8\%$ after 7 d, and were completely degraded after 21 d, in agreement with the palpation-based assessment method. Silanized HA with DS of 21.8% and 40.0%, showed continuous swelling in vivo, reaching $253\% \pm 12\%$ and $163\% \pm 56\%$ after 21 d, respectively. On the contrary, highly silanized HA (DS = 57.7%) did not significantly swell or degrade over the same time period. These results show a tendency similar to that of the in vitro experiments, and demonstrate that the crosslink density determines the in vivo swelling and degradation behavior of Si-HA gels. Interestingly, as compared to in vitro, Si-HA from DS of 21.8% and 40.0% swelled in vivo by a factor of 2.2 and 1.4, respectively. This discrepancy may be attributed to the gelation of Si-HA gels that need a few hours to reach completion (Figure S3, Supporting Information), which may facilitate initial fluid adsorption. To the best of our knowledge, this is the first report describing the use of μ CT for

the rapid evaluation of the volume of explanted hydrogels. This strategy is easy to implement, and allows a precise determination of hydrogel volume. However, it also requires that the hydrogel does not initially contain proteins negatively stained by the opacifying agent (e.g., fibrins, collagens). Altogether, these results demonstrate that the biodegradation rate and swelling profile of in situ forming Si-HA hydrogels can be tuned by controlling the crosslink density.

2.6. Inflammatory Response to Si-HA Hydrogel Implantation

As a final characterization step, we evaluated the biocompatibility of Si-HA hydrogels following in vivo implantation. At 7 and 21 d after hydrogel implantation, the inflammatory response was evaluated by histomorphometric analyses (i.e., type of infiltrate, cell counting, measures of the periprosthetic tissue thickness) on hematoxylin, eosin and Safran (HES)-stained samples. All Si-HA formulations triggered an initial inflammatory response upon injection, characterized at day 7 by a cell population composed of fibroblasts, macrophages, and a few lymphocytes⁽⁶³⁾ (Figure 5A; and Figure S6, Supporting Information). Similar cell densities (≈ 400 cells per Mpixel^2) were observed for all injected formulations (Figure 5B), as well as a thick, but loose, fibroinflammatory capsule (from 64 to 153 μm , for DS = 40.0% and 21.8%) surrounding the materials (Figure 5C). This type of initial inflammatory response is commonly reported for implanted biomaterials, and may result from the injury caused by the

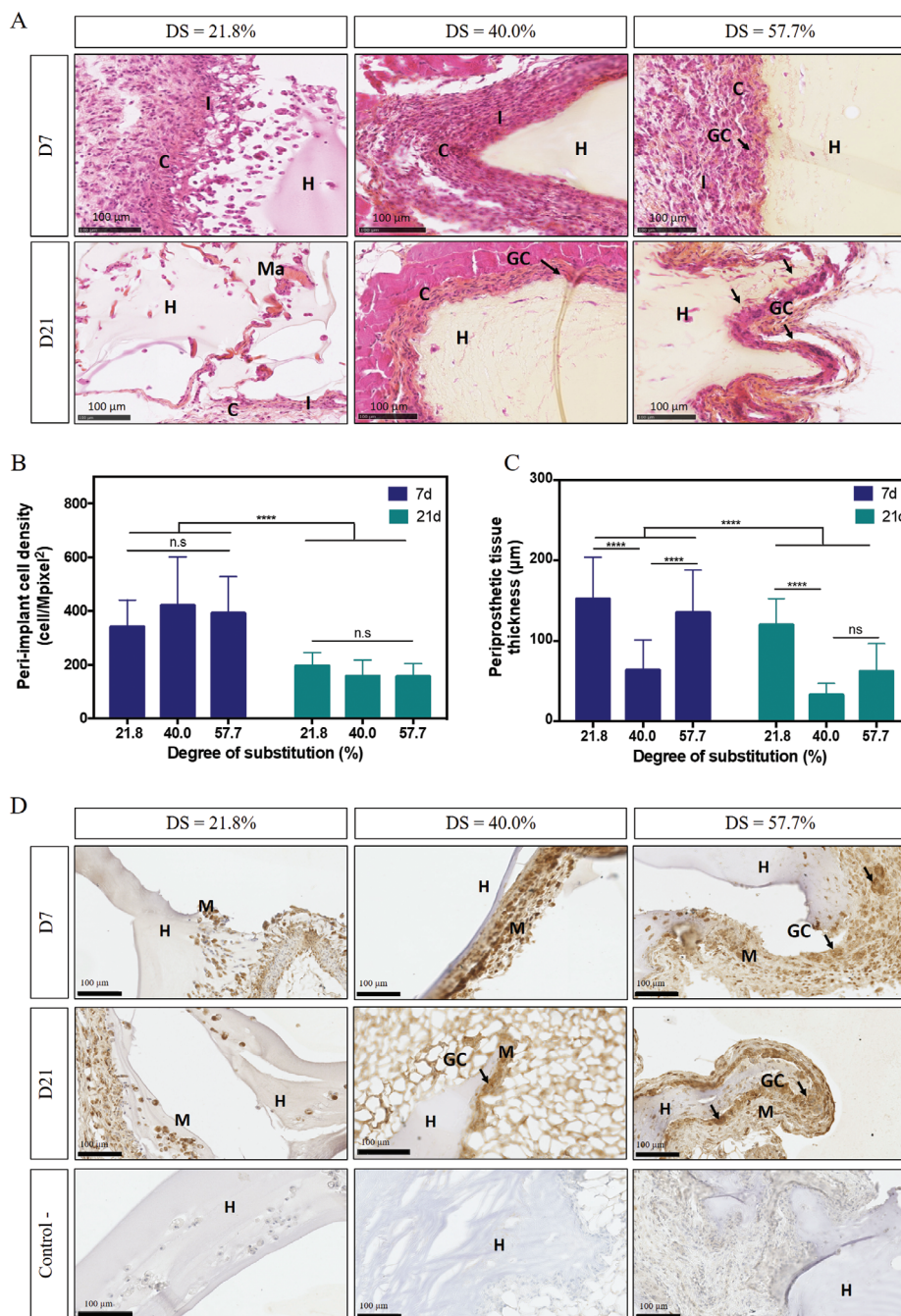


Figure 5. Evaluation of the inflammatory response induced by subcutaneous injections of Si-HA hydrogels. A) Representative histological images of Si-HA hydrogels with DS of 21.8%, 40.0%, and 57.7%, using HES staining, 7- and 21-days postinjection. H: hydrogel, C: capsule, Ma: collagenous matrix, I: inflammatory infiltrate, GC: giant cells. B) Quantification of the peri-implant cell density. C) Evaluation of the thickness of the periprosthetic tissue surrounding Si-HA hydrogels, 7- and 21-days postinjection. D) Representative immunohistological staining of the pan-macrophage marker CD68 and the negative control, after 7 and 21 d. Positive CD68⁺ macrophages are stained in brown. Cell nuclei and hydrogels are stained in blue. Black arrows indicate giant cells. H: hydrogel, M: macrophages, GC: giant cells. Data are represented as mean ± SD, *n* = 3 mice with 3 random fields per mouse. Statistical significance B,C) was evaluated using a two-way ANOVA with a Tukey's multiple comparison test (ns: not significant, *****p* < 0.0001).

injection procedure.^[63–65] Infiltrated cells were also noticed within Si-HA gels with DS of 13.5% and 21.8%, whereas highly silanized HA (DS = 40.0% and 57.7%) showed limited to no cell infiltration. Consistent with these observations, Ehrbar et al. noticed in vivo cell infiltration in low-density polyethylene gly-

col gels, which was otherwise inhibited in stiffer networks.^[66] Si-HA gels have a theoretical mesh size smaller than the typical diameter of a cell (i.e., 1–20 μm), and result from the formation of irreversible covalent bonds. Thus, cell infiltration is probably driven by the erosion mechanism of the gel, as previously

observed for similar systems.^[67] In low-silanized gels, rapid enzyme and water uptake and subsequent bulk erosion of the gel occurs, facilitating cell infiltration. Conversely, the limited diffusivity of highly silanized HA gels only allows for surface erosion, which ultimately impairs cell infiltration. After 21 d, no polymorphonuclear cells could be detected, indicative of a resorption of the acute phase and an absence of pyogenic infection.^[64] No residual inflammation was observed in the fully-degraded samples (DS = 13.5%, Figure S5, Supporting Information), showing that a normal wound healing process occurred after Si-HA degradation. In samples where the hydrogel was still detectable after 21 d, a significant decrease in the peri-implant cell density (from 400 to 200 cells per Mpixel²) was observed, as well as a significant diminution ($p < .0001$) of the periprosthetic fibrous tissue. These results indicate a resorption of the initial inflammation caused by the injection, and highlight the biocompatibility of Si-HA gels. Interestingly, a newly secreted collagenous matrix was observed in the Si-HA gels with a DS of 21.8%, showing that cells are able to colonize the hydrogel. Further immunohistochemical detections of the pan-macrophage marker CD68 revealed the vast majority of infiltrated cells were macrophages, indicating their central role in inducing hydrogel degradation (Figure 5D; and Figure S4, Supporting Information). In the slow-degrading gels (DS = 40.0% and 57.7%), an absence of infiltrated cells was noticed and CD68⁺-macrophages only formed a thin layer around the implants. Some multinucleated giant cells were also visible, indicative of a foreign body reaction typically observed for slow-degrading materials.^[68] In agreement with previous reports,^[63,69] our results suggest that the extent of the foreign body response is correlated to the degradation rate of the hydrogels, and thus to the crosslink density. Although beyond the scope of this article, further investigations of the macrophage polarization to a pro- (M1) or anti- (M2) inflammatory phenotype could be performed to elucidate how the interactions between the material and macrophages influence the inflammatory response.

3. Conclusion

In this study, we successfully designed for the first time in situ forming Si-HA hydrogels using the hybrid inorganic–organic silanization chemistry. By tuning the DS and MW of Si-HA, we showed that single-polymer gels can be formed under physiological conditions of pH and temperature, with tunable gelation time and stiffness. We confirmed the cytocompatibility of Si-HA hydrogels with 3 different cell types (i.e., murine L929 fibroblasts, human BMSCs, and ASCs), and demonstrated their in situ forming ability and biocompatibility. We finally showed that their degradation profiles can be tuned from days to weeks in vivo. Future experiments should evaluate the ability of Si-HA gels to favor tissue regeneration in tissue engineering applications.

4. Experimental Section

Materials: Sodium hyaluronate produced by *Streptococcus equi* with average molecular weights of 332 and 2240 kDa, and dispersities of 2.1 and 1.4, respectively, were provided by HTL S.A.S (France). 2-(N-morpholino)ethanesulfonic acid (MES) and 4-(4,6-dimethoxy-1,3,5-triazin-2-yl)-4-methyl-morpholinium chloride (DMT-MM) were purchased from TCI Europe (Belgium). L929 cells were purchased from ATCC (USA).

Human bone marrow mesenchymal stromal cells (hBMSCs) and Promo-cell special medium were acquired from Promocell (Germany). Hank's balanced salt solution, Dulbecco's Modified Eagle Medium (DMEM), Penicillin/Streptomycin, PBS and the Live/Dead kit were purchased from ThermoFisher Scientific (USA). Fetal bovine serum (FBS) and fetal calf serum were purchased from Dominique Dutscher (France). Ethanol 100% was purchased from VWR (USA). Ketamine (Imalgène 1000) and Xylazine (Rompun) were purchased from Merial (France) and Bayer Medical (Germany), respectively. Otherwise stated, all the other reagents were purchased from Sigma-Aldrich (USA).

Synthesis of Silanized Hyaluronic Acid: Silanized HA (Si-HA) was prepared by amidation of the carboxylic acid functions of HA with 3-aminopropyltriethoxysilane (APTES), using DMT-MM as an activating agent.^[70] Six different conditions were tested, using two molecular weights (332 and 2240 kDa) and increasing equivalents of DMT-MM and APTES (1:1, 2:2 and 4:4). HA (1 g, 2.5 mmol) was first dissolved in 100×10^{-3} M MES (100 mL) for 2 h. After complete dissolution, the DMT-MM reagent (0.69 g (1 eq), 1.38 g (2 eq), 2.76 g (4 eq)) was added for 1 h. Thereafter, APTES (0.58 mL (1 eq), 1.17 g (2 eq), 2.33 g (4 eq)) was added dropwise, and the reaction mixture was kept under vigorous stirring for 24 h at room temperature. The reaction mixture was then dialyzed (MWCO: 6–8 kDa) against NaOH 0.04 N for 18 h followed by deionized water until conductivity reached $10 \mu\text{S cm}^{-1}$. The solution was adjusted with 0.5 M NaCl prior to precipitation in cold ethanol (4 °C). The precipitate was then successively washed with 70 % v/v and 100% v/v ethanol, before drying at 37 °C for 24 h. Each synthesis was repeated three times to ensure repeatability. Silanol-modified HA was characterized by inductively coupled plasma-atomic emission spectroscopy (ICP-AES), ¹H-NMR and SEC (Supporting Information).

Formulation of Si-HA Hydrogels: Si-HA hydrogels with similar polymer content were typically prepared as follows: Si-HA was dissolved at 3.75% w/v in 0.1 N NaOH for 16 h and sterile-filtered using 0.22 μm Millipore filters. The solution was mixed with a sterile-filtered 2-[4-(2-hydroxyethyl)piperazin-1-yl]ethanesulfonic acid (HEPES) buffer using Luer-lock syringes in a 4/1 (solution/buffer) volume ratio, to obtain a final concentration of 3% w/v Si-HA. The buffer composition (336×10^{-3} M HEPES, 300×10^{-3} M NaCl, 0.22 M HCl) was adapted to obtain a final pH of 7.4 and an osmolality of 300 mOsm.

Viscosity Profiles and Zero-Shear Viscosity: Viscosity measurements were performed at 23 °C using a stress-controlled RS300 rheometer (HAAKE, ThermoFisher Scientific, USA) with a cone/plate 60 mm 1° titanium geometry. Viscosity measurements of 3.75% w/v Si-HA solutions were performed in a shear rate range of 0.1–2000 s⁻¹. Flow curves were fitted using the simplified Cross model to determine the zero-shear viscosity.^[71]

Injectability of Si-HA Solutions: The injectability of Si-HA solutions after pH adjustment to 7.4 was assessed by measuring the force required to inject them through a 23G needle. Experiments were performed on a texture analyzer (TAHD⁺, Stable Micro Systems, UK), equipped with a 5 kg load cell, at a rate of 2 mm s⁻¹. Data were recorded on the Exponent Software.

Gelation Time of Si-HA Solutions: The sol–gel transition was determined by performing multiwave frequency sweeps on a stress-controlled RS300 rheometer, using a cone/plate 60 mm 1° titanium geometry. A constant stress of 1 Pa was selected and a range of 5 frequencies (0.1, 0.3, 0.5, 1.3, and 3 Hz) was applied. Experiments were conducted at 37 °C and started immediately after mixing the Si-HA solution with the buffer. The gelation time is determined as the time when the loss tangent, $\tan \delta$, is independent of the frequency.^[71]

Unconfined Compression of Si-HA Hydrogels: Unconfined compression tests were performed on nonswollen cylindrical hydrogels (diameter 6 mm \times height 5 mm) using a texture analyzer TAHD⁺. Compression assays were conducted at a rate of 0.01 mm s⁻¹. All the experiments were performed at room temperature on Si-HA hydrogels crosslinked for 3 d at 37 °C. The elastic modulus (E) was extracted from the slope of the first 10% of the stress versus strain curve.

Swelling and Stability Analysis: The swelling and stability of various Si-HA hydrogel formulations were evaluated by monitoring the mass of 100

μL Si-HA hydrogels over time at 37 °C. Briefly, 100 μL of prehydrogel solutions were rapidly transferred in preweighed, 2 mL Eppendorf tubes, and left at 37 °C 72 h for complete gelation. 900 μL of 1X PBS were added, before incubation at 37 °C. At regular intervals, the supernatants were removed and the samples weighted. The swelling was determined as the ratio of a hydrogel mass at a given time point divided by its initial mass.

In Vitro Enzymatic Degradation: In vitro enzymatic degradation of Si-HA hydrogels was monitored over 40 d, with a similar experimental design to that of the swelling and stability experiment. Hydrogel samples ($n = 9$) were weighted (W_a) and further immersed in 10 U mL^{-1} hyaluronidase IV-S in PBS at 37 °C. At regular intervals, excess PBS was gently removed, and the samples weighted. Fresh hyaluronidase solution was added after every measurement to ensure constant enzymatic activity over time. The degradation was determined as the ratio of a hydrogel mass at a given time point divided by its initial mass.

Cell Culture and 3D Viability Assay: hASCs from lipoaspirates were isolated as previously described (Supporting Information).^[72] L929 cells and hASCs were cultured in DMEM medium supplemented with 10% FBS and 1% penicillin/streptomycin. Human BMSCs were cultured in Promocell special medium supplemented with 1% penicillin/streptomycin. The medium was changed every 2–3 d. hASCs and hBMSCs were used between passage 2 and 4. To evaluate the cytocompatibility of Si-HA hydrogels, the three cell types were independently passaged and suspended in 50 μL of DMEM at a concentration of 10^6 cells mL^{-1} . In parallel, 3% w/v Si-HA hydrogels (DS = 13.5%, 21.8%, 40.0%, and 57.7%) were prepared as described above. After homogeneously mixing the Si-HA solution with the HEPES buffer, cells were added to the mixture using a pipette, mixed again using Luer-lock syringes, and transferred to Transwell inserts (200 μL per insert). The hydrogels were left for crosslinking for 45 min at 37 °C before adding fresh medium. Cell viability within Si-HA hydrogels was assessed by Live/dead assay after 1, 3, and 7 d. Actinomycin ($5 \mu\text{g mL}^{-1}$) was used as a positive control for cell death. Images were recorded by confocal imaging (Nikon, Japan). Cell viability was calculated as the number of living cells divided by the total cell number.

To evaluate if the injection process through Si-HA precursor solutions is not detrimental to cell viability, hASCs were mixed with Si-HA precursor solutions as described above. After 1 min, the cell-containing precursor solutions were injected through a 23 G needle into Transwell inserts. After 2 h, cell viability was assessed by a Live/dead assay as described above.

In Vivo Injections of Si-HA Gels: 12 female C57BL/6 mice (aged 12 weeks) were purchased from Charles River (USA). All the procedures involving the use of animals were in accordance with the Medical Animal Care Guidelines of the University of Nantes (Ethical number: Apafis 12838). Sterile 3% w/v Si-HA hydrogels (DS = 13.5%, 21.8%, 40.0%, and 57.7%) were prepared as described above under aseptic conditions. 250 μL of each of the four Si-HA solutions tested (DS = 13.5%, 21.8%, 40.0%, and 57.7%) were subcutaneously injected in the back of each mouse. The gel injections were performed under general anesthesia obtained by a single injection of Ketamine/Xylazine. After 7 and 21 d, mice were euthanized by CO_2 inhalation, and hydrogels were collected before fixation in 4% w/v paraformaldehyde for 48 h.

Volume Determination by MicroCT: Samples were soaked overnight at 4 °C in a 2% w/v solution of phosphotungstic acid, used as a contrast agent of collagen proteins. Microcomputed tomography (μCT) analyses were performed on a Skyscan 1272 X-ray Micro-CT (Bruker, USA) to determine the volume of Si-HA hydrogels. Acquisitions were performed at a spatial resolution of 20 μm , with a rotation step of 0.7°. A 1 mm thick aluminum filter was used (voltage: 80 kV; current: 125 μA ; frame averaging: 3). 3D reconstructions were performed using the NRecon software, and post-treated with the CTan software to determine a volume of interest. As HA hydrogels were not stained by the phosphotungstic acid, their respective volume was determined by calculating the area without staining. The volumetric ratio was then calculated as the ratio between the volume at a given time and the initial volume injected (250 μL).

Histological Analyses: Samples were embedded in paraffin wax and sectioned (5 μm thick). Tissue samples were stained with HES. Stained sections were recorded on a whole slide imager (Nanozoomer Hamamatsu, Japan) and visualized with the NDPview2 software. Direct thick-

ness measurements of the fibrotic capsule were performed on tissue samples (10 measures/sample) using the NDPview2 software.

Statistical Analysis: All the data are presented as mean \pm standard error. Otherwise specified, all experiments were performed for $n = 3$ samples. Comparison between two normally distributed data sets were performed by a Student unpaired t -test. Comparison between multiple normally distributed data sets were performed by one-ANOVA coupled with a posthoc Tukey's multiple comparison test. Comparison between multiple normally distributed data sets and multiple time points were performed using a two-way ANOVA coupled with a posthoc Tukey's multiple comparison test. For all experiments, significance levels were set at * $p < 0.05$, ** $p < 0.01$, *** $p < 0.001$, **** $p < 0.0001$. Statistical analysis was carried out using GraphPad Prism 8.2.0 software (GraphPad Software Inc., USA).

Supporting Information

Supporting Information is available from the Wiley Online Library or from the author.

Acknowledgements

K.F., C.T., V.D., H.G., and P.W. contributed equally to this work. The authors acknowledge the UTE-IRS-UN Animal Facility, MicroPiCell imaging facility, and SC3M Histology facility of the SFR Santé F Bonamy (UMS INSERM 016/CNRS 3556) (Nantes, France) for their technical support. They acknowledge Constance Lesage who performed the video showing the formation of Si-HA gels. They also acknowledge the support of HTL S.A.S and the Association Nationale de la Recherche et de la Technologie (Grant No. 2015-1080).

Conflict of Interest

K.F., L.M., D.D., P.B., and A.B. are members of the HTL S.A.S company.

Keywords

biodegradability, hyaluronic acid, hydrogels, silanization, tissue engineering

Received: June 9, 2020

Revised: August 9, 2020

Published online:

- [1] A. S. Hoffman, *Adv. Drug Delivery Rev.* **2012**, *64*, 18.
- [2] A. M. Rosales, K. S. Anseth, *Nat. Rev. Mater.* **2016**, *1*, 15012.
- [3] S. R. Caliani, J. A. Burdick, *Nat. Methods* **2016**, *13*, 405.
- [4] B. A. Aguado, W. Mulyasmita, J. Su, K. J. Lampe, S. C. Heilshorn, *Tissue Eng., Part A* **2012**, *18*, 806.
- [5] J.-A. Yang, J. Yeom, B. W. Hwang, A. S. Hoffman, S. K. Hahn, *Prog. Polym. Sci.* **2014**, *39*, 1973.
- [6] S. Hou, X. Wang, S. Park, X. Jin, P. X. Ma, *Adv. Healthcare Mater.* **2015**, *4*, 1491.
- [7] A. A. Foster, L. M. Marquardt, S. C. Heilshorn, *Curr. Opin. Chem. Eng.* **2017**, *15*, 15.
- [8] C. B. Rodell, M. E. Lee, H. Wang, S. Takebayashi, T. Takayama, T. Kawamura, J. S. Arkes, N. N. Dusan, S. M. Dorsey, W. R. T. Witschey, J. J. Pilla, J. H. Gorman III, J. F. Wenk, J. A. Burdick, R. C. Gorman, *Circ.: Cardiovasc. Interventions* **2016**, *9*, e004058.
- [9] S. E. Gullbrand, T. P. Schaer, P. Agarwal, J. R. Bendigo, G. R. Dodge, W. Chen, D. M. Elliott, R. L. Mauck, N. R. Malhotra, L. J. Smith, *Acta Biomater.* **2017**, *60*, 201.

- [10] K. Shi, B. Xue, J. Liao, Y. Qu, Z. Qian, *Mater. Express* **2017**, *7*, 417.
- [11] E. Bakaic, N. M. B. Smeets, T. Hoare, *RSC Adv.* **2015**, *5*, 35469.
- [12] K. Flégeau, R. Pace, H. Gautier, G. Rethore, J. Guicheux, C. Le Visage, P. Weiss, *Adv. Colloid Interface Sci.* **2017**, *247*, 589.
- [13] V. Delplace, P. E. B. Nickerson, A. Ortin-Martinez, A. E. G. Baker, V. A. Wallace, M. S. Shoichet, *Adv. Funct. Mater.* **2020**, *30*, 1903978.
- [14] T. Montheil, C. Echalié, J. Martinez, G. Subra, A. Mehdi, *J. Mater. Chem. B* **2018**, *6*, 3434.
- [15] X. Bourges, P. Weiss, G. Daculsi, G. Legeay, *Adv. Colloid Interface Sci.* **2002**, *99*, 215.
- [16] C. Trojani, F. Boukhechba, J.-C. Scimeca, F. Vandebos, J.-F. Michiels, G. Daculsi, P. Boileau, P. Weiss, G. F. Carle, N. Rochet, *Biomaterials* **2006**, *27*, 3256.
- [17] F. Hached, C. Vinatier, P.-G. Pinta, P. Hulin, C. Le Visage, P. Weiss, J. Guicheux, A. Billon-Chabaud, G. Grimandi, *Stem Cells Int.* **2017**, *2017*, 9303598.
- [18] C. Vinatier, D. Magne, A. Moreau, O. Gauthier, O. Malard, C. Vignes-Colombeix, G. Daculsi, P. Weiss, J. Guicheux, *J. Biomed. Mater. Res., Part A* **2007**, *80A*, 66.
- [19] E. Mathieu, G. Lamirault, C. Toquet, P. Lhomme, E. Rederstorff, S. Sourice, K. Bateau, P. Hulin, V. Forest, P. Weiss, J. Guicheux, P. Lemarchand, *PLoS One* **2012**, *7*, e51991.
- [20] L. Moussa, C. Demarquay, G. Réthoré, M. A. Benadjouad, F. Siñeriz, G. Pattapa, J. Guicheux, P. Weiss, D. Barritault, N. Mathieu, *Sci. Rep.* **2019**, *9*, 164.
- [21] E. Rederstorff, P. Weiss, S. Sourice, P. Pilet, F. Xie, C. Siquin, S. Collic-Jouault, J. Guicheux, S. Laib, *Acta Biomater.* **2011**, *7*, 2119.
- [22] B. H. Fellah, P. Weiss, O. Gauthier, T. Rouillon, P. Pilet, G. Daculsi, P. Layrolle, *J. Orthop. Res.* **2006**, *24*, 628.
- [23] K. S. Girish, K. Kemparaju, *Life Sci.* **2007**, *80*, 1921.
- [24] C. Guo, L. Sun, H. Cai, Z. Duan, S. Zhang, Q. Gong, K. Luo, Z. Gu, *ACS Appl. Mater. Interfaces* **2017**, *9*, 23508.
- [25] M. I. Tammi, A. J. Day, E. A. Turley, *J. Biol. Chem.* **2002**, *277*, 4581.
- [26] X.-H. Bian, G.-Y. Zhou, L.-N. Wang, J.-F. Ma, Q.-L. Fan, N. Liu, Y. Bai, W. Guo, Y.-Q. Wang, G.-P. Sun, P. He, X. Yang, X.-S. Su, F. Du, G.-F. Zhao, J.-N. Miao, L. Ma, L.-Q. Zheng, D.-T. Li, J.-M. Feng, *Kidney Blood Pressure Res.* **2013**, *38*, 11.
- [27] M. Litwiniuk, A. Krejner, M. S. Speyrer, A. R. Gauto, T. Grzela, *Wounds Compend. Clin. Res. Pract.* **2016**, *28*, 78.
- [28] A. Fallacara, E. Baldini, S. Manfredini, S. Vertuani, *Polymers* **2018**, *10*, 701.
- [29] H.-Y. Lee, H.-E. Kim, S.-H. Jeong, *Colloids Surf., B* **2019**, *174*, 308.
- [30] D. A. Sánchez-Téllez, L. M. Rodríguez-Lorenzo, L. Téllez-Jurado, *Carbohydr. Polym.* **2020**, *230*, 115590.
- [31] C. Vinatier, O. Gauthier, A. Fatimi, C. Merceron, M. Masson, A. Moreau, F. Moreau, B. Fellah, P. Weiss, J. Guicheux, *Biotechnol. Bioeng.* **2009**, *102*, 1259.
- [32] P. M. Chichirico, R. Riva, J.-M. Thomassin, J. Lesoeur, X. Struillou, C. Le Visage, C. Jérôme, P. Weiss, *Dent. Mater.* **2018**, *34*, 1769.
- [33] J. A. Burdick, C. Chung, X. Jia, M. A. Randolph, R. Langer, *Biomacromolecules* **2005**, *6*, 386.
- [34] T. Hardingham, *Chemistry and Biology of Hyaluronan*, Elsevier, Oxford **2004**.
- [35] J. Kiss, in *Advances in Carbohydrate Chemistry and Biochemistry* (Eds: R. S. Tipson, D. Horton), Academic Press, New York **1974**, pp. 229–303.
- [36] R. Stern, G. Kogan, M. J. Jedrzejewski, L. Soltés, *Biotechnol. Adv.* **2007**, *25*, 537.
- [37] I. Gatej, M. Popa, M. Rinaudo, *Biomacromolecules* **2005**, *6*, 61.
- [38] G. Alonci, F. Fiorini, P. Riva, F. Monroy, I. López-Montero, S. Perretta, L. De Cola, *ACS Appl. Bio Mater.* **2018**, *1*, 1301.
- [39] D. Kalladka, J. Sinden, K. Pollock, C. Haig, J. McLean, W. Smith, A. McConnachie, C. Santosh, P. M. Bath, L. Dunn, K. W. Muir, *Lancet* **2016**, *388*, 787.
- [40] V. Burckbuchler, G. Mekhloufi, A. P. Giteau, J. L. Grossiord, S. Huille, F. Agnely, *Eur. J. Pharm. Biopharm.* **2010**, *76*, 351.
- [41] E. B. Dolan, L. Kovarova, H. O'Neill, M. Pravda, R. Sulakova, I. Scigalkova, V. Velebny, D. Daro, N. Braun, G. M. Cooney, S. Straino, B. L. Cavanagh, A. Flanagan, H. M. Kelly, G. P. Duffy, B. P. Murphy, *J. Biomater. Appl.* **2018**, *33*, 681.
- [42] W. Cao, J. Sui, M. Ma, Y. Xu, W. Lin, Y. Chen, Y. Man, Y. Sun, Y. Fan, X. Zhang, *J. Mater. Chem. B* **2019**, *7*, 4413.
- [43] D. Bermejo-Velasco, A. Azémar, O. P. Oommen, J. Hilborn, O. P. Varghese, *Biomacromolecules* **2019**, *20*, 1412.
- [44] M. Patenaude, S. Campbell, D. Kinio, T. Hoare, *Biomacromolecules* **2014**, *15*, 781.
- [45] K. H. Vining, D. J. Mooney, *Nat. Rev. Mol. Cell Biol.* **2017**, *18*, 728.
- [46] R. G. Wells, *Hepatology* **2008**, *47*, 1394.
- [47] A. J. Engler, S. Sen, H. L. Sweeney, D. E. Discher, *Cell* **2006**, *126*, 677.
- [48] T. Canal, N. A. Peppas, *J. Biomed. Mater. Res.* **1989**, *23*, 1183.
- [49] M. S. Hahn, H. Liao, D. Munoz-Pinto, X. Qu, Y. Hou, M. A. Grunlan, *Acta Biomater.* **2008**, *4*, 1161.
- [50] D. N. Shah, S. Recktenwall-Work, K. S. Anseth, *Biomaterials* **2008**, *29*, 2060.
- [51] F. van de Manacker, K. Braeckmans, N. el Morabit, S. C. De Smedt, C. F. van Nostrum, W. E. Hennink, *Adv. Funct. Mater.* **2009**, *19*, 2992.
- [52] J. Li, D. J. Mooney, *Nat. Rev. Mater.* **2016**, *1*, 16071.
- [53] Y. Gao, W. Kong, B. Li, Y. Ni, T. Yuan, L. Guo, H. Lin, H. Fan, Y. Fan, X. Zhang, *Colloids Surf., B* **2018**, *167*, 448.
- [54] H. Lopez Hernandez, A. K. Grosskopf, L. M. Stapleton, G. Agmon, E. A. Appel, *Macromol. Biosci.* **2019**, *19*, 1800275.
- [55] X.-T. He, R.-X. Wu, X.-Y. Xu, J. Wang, Y. Yin, F.-M. Chen, *Acta Biomater.* **2018**, *71*, 132.
- [56] S. Wang, F. Taraballi, L. P. Tan, K. W. Ng, *Cell Tissue Res.* **2012**, *347*, 795.
- [57] A. Blaeser, D. F. Duarte Campos, M. Weber, S. Neuss, B. Theek, H. Fischer, W. Jahnen-Dechent, *BioRes. Open Access* **2013**, *2*, 374.
- [58] M. H. Amer, L. J. White, K. M. Shakesheff, *J. Pharm. Pharmacol.* **2015**, *67*, 640.
- [59] A. Ferrini, M. M. Stevens, S. Sattler, N. Rosenthal, *Front. Cardiovasc. Med.* **2019**, *6*, 26.
- [60] S. Guo, X. Wang, Y. Dai, X. Dai, Z. Li, Q. Luo, X. Zheng, Z. Gu, H. Zhang, Q. Gong, K. Luo, *Adv. Sci.* **2020**, *7*, 2000467.
- [61] H. Cai, X. Dai, X. Wang, P. Tan, L. Gu, Q. Luo, X. Zheng, Z. Li, H. Zhu, H. Zhang, Z. Gu, Q. Gong, K. Luo, *Adv. Sci.* **2020**, *7*, 1903243.
- [62] B. Reid, M. Gibson, A. Singh, J. Taube, C. Furlong, M. Murcia, J. Elisseoff, *J. Tissue Eng. Regen. Med.* **2015**, *9*, 315.
- [63] K. Jones, in *Host Response to Biomaterials* (Ed.: S. F. Badylak), Academic Press, Oxford **2015**, pp. 189–237.
- [64] J. M. Anderson, A. Rodriguez, D. T. Chang, *Semin. Immunol.* **2008**, *20*, 86.
- [65] J. M. Morais, F. Papadimitrakopoulos, D. J. Burgess, *AAPS J.* **2010**, *12*, 188.
- [66] M. Ehrbar, A. Sala, P. Lienemann, A. Ranga, K. Mosiewicz, A. Bittermann, S. C. Rizzi, F. E. Weber, M. P. Lutolf, *Biophys. J.* **2011**, *100*, 284.
- [67] T. R. Ham, R. T. Lee, S. Han, S. Haque, Y. Vodovotz, J. Gu, L. R. Burnett, S. Tomblin, J. M. Saul, *Biomacromolecules* **2016**, *17*, 225.
- [68] W. Kenneth Ward, *J. Diabetes Sci. Technol.* **2008**, *2*, 768.
- [69] R. Censi, S. van Putten, T. Vermonden, P. di Martino, C. F. van Nostrum, M. C. Harmsen, R. A. Bank, W. E. Hennink, *J. Biomed. Mater. Res., Part A* **2011**, *97A*, 219.
- [70] P. Weiss, J. Guicheux, E. Rederstorff, S. Laib, G. Rethore, (Silylated Biomolecules), WO2011089267 A1, **2011**.
- [71] A. Fatimi, J. F. Tassin, S. Quillard, M. A. V. Axelos, P. Weiss, *Biomaterials* **2008**, *29*, 533.
- [72] C. Merceron, S. Portron, C. Vignes-Colombeix, E. Rederstorff, M. Masson, J. Lesoeur, S. Sourice, C. Siquin, S. Collic-Jouault, P. Weiss, C. Vinatier, J. Guicheux, *Stem Cells* **2012**, *30*, 471.